Towards Full Electrification: Virtual Thermal Prototyping of a Dual-Mode Electro-Hydrostatic Actuator for a Hybrid Wheel Loader

Baoyan Hu[1,*], Chao Wang[1], and Jian Fu[1]

1. School of Mechanical Engineering and Automation, Beihang University, Beijing, P.R China
E-mail: buaahby@outlook.com, wangchaoo@buaa.edu.cn, fujian@buaa.edu.cn
*School of Mechanical Engineering and Automation, Beihang University, Beijing, P.R China

Abstract

The shift from traditional diesel-powered machinery to more environmentally-friendly alternatives in the non-road mobile machinery sector is driven by strict environmental regulations and the demand for greater efficiency. While hybrid solutions have demonstrated benefits such as improved fuel efficiency and reduced emissions, the electrification of hydraulic actuation systems has received less attention. This study introduces a dual-mode electro-hydrostatic actuator designed to replace the hydraulic lift cylinder in hybrid wheel loaders, addressing challenges in efficiency, safety, and thermal management. The actuator operates in two distinct modes: a typical mode and a safety mode employing counterbalance valves, which enhances load-lowering control and safety through integrated solenoid valves and counterbalance mechanisms. Using co-simulation between AMESim and MATLAB/Simulink, the dynamic performance and thermal behavior of the electro-hydrostatic actuator are evaluated over a 3600 second duty cycle. Simulation results highlight differences in thermal and dynamic performance between the two modes. The safety mode achieves superior load-holding capability with reduced motor current demand but experiences higher temperatures in the cylinder and valves due to discontinuous fluid flow. Conversely, the typical mode encounters greater thermal stress in the pump, particularly at the leakage point. This work provides a detailed analysis of the thermal behavior of the electro-hydrostatic actuator, offering crucial insights for optimizing thermal design and cooling strategies. The study also contributes to the advancement of electrified hydraulic systems and integrating hybrid powertrains with electrified hydraulic systems, paving the way for sustainable, high-performance non-road mobile machinery solutions that meet safety and operational standards.

Keywords: thermal behavior, hybrid wheel loader, electrification, electro-hydrostatic actuator, counterbalance valve

1 Introduction

The transition toward full electrification of non-road mobile machinery (NRMM) is driven by increasingly strict environmental regulations and the rising demand for sustainable technologies[1]. Conventional diesel-powered NRMM confronts challenges such as high emissions and inefficiencies, necessitating innovative solutions. Hybrid powertrains are emerging as practicable alternatives, offering enhanced fuel efficiency, reduced emissions, improved operational performance, lower noise levels, and reduced maintenance costs[2]. Significant research has explored various hybrid powertrains, the focus has primarily been on powertrains[3]. For instance, [4], [5], [6] introduces three hybrid powertrains developed by different original equipment manufacturers (OEMs): 1. series 2. parallel 3. series-parallel. However, OEMs retain initial hydraulic circuits that possess system inherent power losses (SIPL).

Besides, limited attention is given to the electrification of hydraulic actuation systems. Two concepts, individual metering system and secondary control using hydraulic transformer are contributions to the improvement of hydraulic actuation systems. Although individual metering system lowers the energy consumption, SIPL still exists when loads are in different weights[7]. Hydraulic transformer is one of valve-less systems that avoids SIPL, but the increased number of hydraulic components and unchanged hydraulic power supply bring issues of more required space and higher costs[8]. Electro-hydrostatic actuators (EHAs) and electro-mechanical actuators (EMAs) are among the promising technologies to address this gap, providing opportunities to improve hybrid NRMM efficiency and enable progress toward full electrification. One of them, EHA, its essential concept is to connect an electrical-motor-controlled pump to a hydraulic cylinder, realizing varied transmission of power. The servo valve is not required in this scheme and thus the power loss across it can be decreased sharply[9]. Because EHA has the potential to recover energy[10], many scholars started to research its application on NRMM. [11] and [12] proposes specific and independent electrified working hydraulic system by adopting direct-driven hydraulics or EHAs. In [13], the researchers incline their work towards how to evaluate the match level between novel actuators and NRMM. Nevertheless, these papers related to adopting EHAs only take functional compatibility into account. In fact, key factors such as physical characteristics, dynamic performance, and compliance with safety standards like ISO 8643[14]—which regulates load-lowering control in case of hydraulic line failure happening in earth-moving machinery—must be considered as well before EHA is implemented on NRMM for real. Additionally, integrated EHA systems face unique challenges in managing heat due to limited space for heat exchangers[15], making thermal analysis essential. Energy is dissipated through heat conduction, convective heat transfer, and radiative heat transfer as passive outputs, which are not considered effective dissipation mechanisms[16]. Moreover, elevated temperatures have a significant impact on the performance of the EHA [17]. [18], [19], [20] have studied the temperature and efficiency of different EHAs by building models or doing experiments. Nonetheless, dynamic performance and thermal behavior of the EHA cannot be observed at the same time via their models.

Therefore, a tool is needed to simultaneously monitor the dynamic performance and thermal behavior of the EHA that satisfies safety standards, enabling its evaluation for potential implementation in hybrid NRMM. This paper introduces an innovative prototype of an integrated EHA designed to replace the lift cylinder in a hybrid wheel loader. This EHA is equipped with counterbalance valves (CBVs) that could be seen as a kind of lowering control devices which ISO 8643 requires to enhance load control and safety while a hybrid wheel loader is working in the safety mode. Furthermore, it also offers an alternative operating mode without CBVs by energizing solenoid valves, which is called typical mode as normal EHA scheme. Naturally, the EHA under safety mode requires more hydraulic power to open the CBVs, making it less energy-efficient compared to the typical mode. However, ISO 8643 mandates the inclusion of lowering control devices in wheel loaders to avoid hazard. Therefore, comparing the performance differences between the two operating modes is both relevant and meaningful for ensuring regulatory compliance. EHA with dual modes also possesses varied heat transfer mechanisms, including the impact of convective cooling in the pump and accumulator in safety mode and the elevated thermal stress on components in typical mode. In order to investigate the specific EHA's thermal behavior and dynamic performance under dual operating modes, co-simulation via MATLAB/Simulink and AMESim is deployed.

This study not only advances understanding of EHA technology but also provides a pathway for high-performance and sustainable hydraulic actuation systems that meet safety and operational standards, offering valuable guidance for the effective implementation of electrified hydraulic systems in hybrid wheel loaders.

The rest of the paper is organized as follows: Section II analyzes heat transfer in the EHA; Section III presents mathematical thermal models based on the lumped-parameter method (LPM); Section IV shows temperature results from a 3600-second duty cycle; Section V discusses the simulation results; Section VI offers conclusions.

2 Heat transfer analysis

EHA system's configuration is given in 2.1, having great influence on analyzing heat transfer. Thermal network models are illustrated to characterize the heat transfer mechanisms within the EHA system in 2.2.

2.1 EHA system

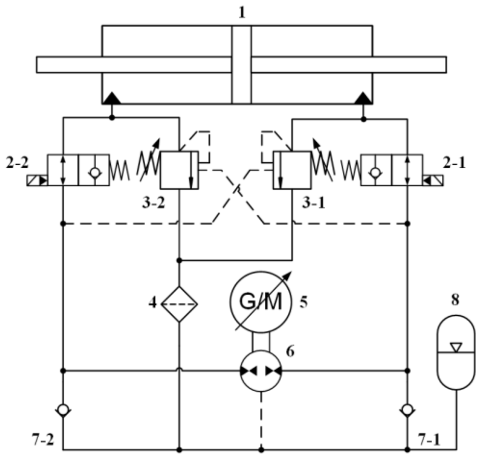

1-symmetric cylinder 2-solenoid valves 3-counterbalance valves 4-filter 5-PMSM 6-axial piston pump/motor 7-check valves 8-accumulator

Figure 1: Schematic diagram of EHA prototype

Figure. 1 shows the schematic diagram of an integrated EHA prototype. The system is built around a symmetric hydraulic cylinder (1), with one of its rods concealed within the housing. The EHA operates in two modes, triggered by the configuration of the two solenoid valves (2):

Typical Mode: In this typical volume-controlled EHA operation, oil flows directly through both solenoid valves, allowing standard actuation. CBVs (3) act as relief valves for safety. It takes the advantage that the system can realize the more accurate and rapider position control. Compared to safety mode, there is a degradation in system security. This mode serves as the baseline for observing the system's behavior when an EHA with a fundamental structure is directly integrated into a wheel loader.

Safety Mode: Solenoid valves operate as check valves, enabling oil to pass through CBVs. This mode directs the fluid flow into the accumulator (8), through the check valves (7), and then to the suction port of the pump/motor (6). This design prevents oil from flowing directly to the inlet of the pump. During load-lowering control, if a pipeline failure occurs, CBVs can shut off the flow to prevent the load from descending uncontrollably, thereby mitigating the risk of accidents and significantly enhancing system safety. However, this comes at the cost of reduced control precision and response speed. This mode provides insight into the system's behavior when the EHA is equipped with CBVs.

The hydraulic circuit includes additional components for functionality and efficiency: a filter (4) for fluid cleanliness, an axial piston pump/motor (6), and a permanent magnet synchronous motor (PMSM) (5), which drives the pump via a coupling. Notably, the pump is immersed in the accumulator, providing a compact and integrated design. The accumulator (8) stores energy and helps smooth operation. This configuration offers enhanced flexibility and allows for detailed studies of performance differences between the two operating modes.

2.2 Heat transfer within EHA

The EHA system comprises components involved in heat transfer, including the cylinder (1), solenoid valves (2), CBVs (3), PMSM (5), pump (6) and accumulator (8). Due to dual operating modes, heat transfer mechanisms and thermal network models differ, as shown in fig. 2 and fig. 3. No matter how the pump rotates, in a clockwise direction or a counterclockwise direction, the direction of the heat transfer is always defined by fig. 2 and fig. 3. Circular nodes represent fluid nodes, while rectangular nodes indicate solid nodes. The pump has four nodes, with mechanical losses at the outlet node and churning losses at the leakage node. In typical mode, convective heat transfer happens between the pump shell and accumulator via direct oil contact. The cylinder and solenoid valves are modeled with three nodes each, with mechanical losses distributed to the cylinder inlet node and outlet node, and valve's energy losses at the outlet node. Heat exchange with external environment occurs at the shells of the cylinder, accumulator, and PMSM via convection and radiation. In safety mode, a CBV replaces one solenoid valve, altering heat transfer pathways and facilitating heat transfer from the CBV to the accumulator as depicted in fig. 3.

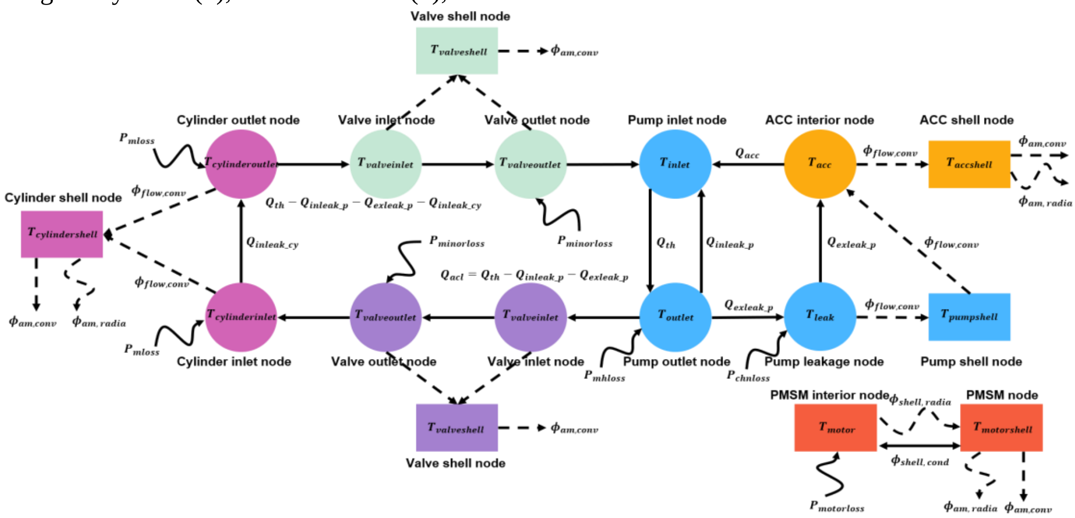

Figure 2: Heat transfer in typical mode based on LPM

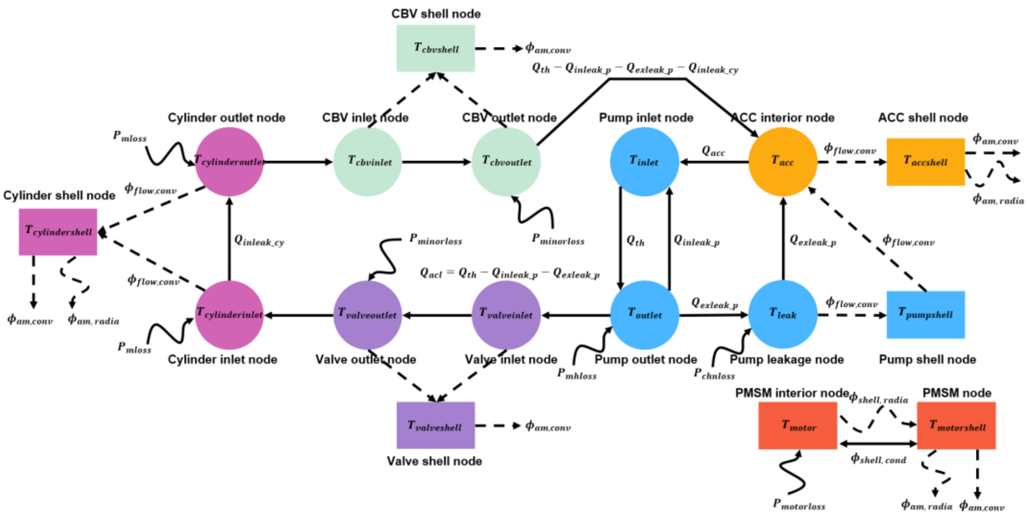

Figure 3: Heat transfer in safety mode based on LPM

3 Thermal modelling

For lumped parameter method and one-dimensional flow, there is a simplified representation of the temperature differential equation. Several authors have presented thermal models of hydraulic systems, for example, referring to [21] for details. In this paper, thermal models are derived from the principles of conservation of energy and mass.

3.1 Basic equation building for different systems

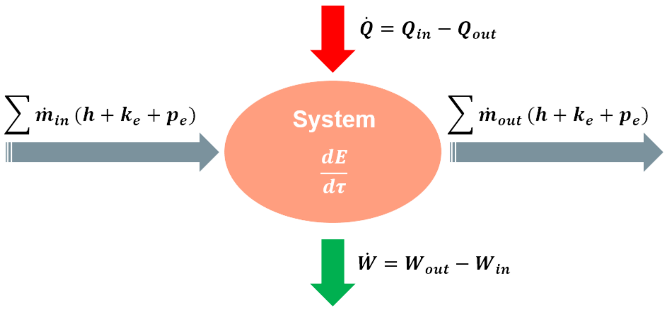

Figure 4: The First law of thermodynamics

Building thermal models must be based on the first law of thermodynamics that is illustrated by fig. 4. There are three primary types of thermodynamic systems categorized by how this system exchanges mass and energy with its surroundings, referring to open systems, closed systems and isolated systems. As shown in fi. 1, cylinder (1), solenoid valves (2), CBVs (3), pump (6) and accumulator (8) belong to open systems, which means that these components exchange energy as well as mass with surroundings. Therefore, an open system should also obey the law of conservation of mass, analyzed through control volume method. PMSM (6) is a kind of closed systems because no mass crosses the boundary of this system, analyzed through control mass method.

For open systems, the temperature differential equation with respect to time has been previously derived in [21]. In this study, the same equation is obtained using an alternative approach. The temperature differential equation is directly presented as follows:

$$\frac{dT}{d\tau} = \frac{1}{c_p m} * \left\{ \begin{array}{c} \sum \dot{m}_{in}\left[c_p(T_{in} - T_{out}) + (1 - \bar{T}\alpha_V)\bar{v}(p_{in} - p_{out})\right] \\ +\dot{Q} - \dot{W}_s + mT\alpha_V v\frac{dp}{d\tau} \end{array} \right\} \tag{1}$$

To enhance the clarity of this equation, the last term within the curly brackets should be extracted separately, as it explicitly represents the effect of pressure variation on temperature change. Apart from this term, the remaining components influence temperature at a given pressure.

Equation (1) is derived based on the assumption that the enthalpy within the control volume is equal to the enthalpy leaving the system. However, this assumption is not practical to all hydraulic components in EHA. Therefore, it is essential to understand the derivation of eq. (1). which is presented in eq. (2):

$$\frac{dT}{d\tau} = \frac{1}{c_p m} * \left\{ \begin{array}{c} \sum \dot{m}_{in}\left[c_p(T_{in} - T) + (1 - T\alpha_V)v_{in}(p_{in} - p)\right] \\ + \sum \dot{m}_{out}\left[c_p(T - T_{out}) + (1 - T\alpha_V)v_{out}(p - p_{out})\right] \\ +\dot{Q} - \dot{W}_s + mT\alpha_V v\frac{dp}{d\tau} \end{array} \right\} \tag{2}$$

For closed systems, the energy equation is quite simpler than that for open systems:

$$\dot{Q} - \dot{W} = \frac{dE_{CM}}{d\tau} \tag{3}$$

Similarly, dE_{CM} is the differential element of the internal energy of this control mass. No mass changes in closed systems, so the term on the right side of the equal sign can be expressed as:

$$\frac{dE_{CM}}{d\tau} = \frac{dU}{d\tau} = \frac{dmu}{d\tau} = m\frac{du}{d\tau} \tag{4}$$

where introduces another thermodynamics property, c_v, which means the specific heat at constant volume. Therefore, the temperature differential equation for the closed system is:

$$\frac{dT}{d\tau} = \frac{1}{c_v m}(\dot{Q} - \dot{W}) \tag{5}$$

3.2 Thermal models of components

Expressions of temperature differential equations on the basis of heat transfer in fig. 2 are as the followings.

The symmetric cylinder (1) in fig. 1 includes 1-inlet node, 1-outlet node and 1-shell node, following the eq. (6-8) respectively:

$$\frac{dT_{cylinderinlet}}{d\tau} = \frac{1}{c_{cylinder} m_{cylinderinlet}} * \left\{ \begin{array}{c} \rho_{oil}\left(Q_{th} - Q_{inleak_p} - Q_{exleak_p}\right) \\ \left[\begin{array}{c} c_{cylinder}\left(T_{valveoutlet} - T_{cylinderinlet}\right) \\ +\left(1 - \frac{\alpha_V\left(T_{cylinderinlet} + T_{valveoutlet}\right)}{2}\right) \\ * \bar{v}\left(p_{valveoutlet} - p_{cylinderinlet}\right) \end{array} \right] \\ -h_{cylindershell}A_{cylinderinlet}\left(T_{cylinderinlet} - T_{cylindershell}\right) \\ +P_{mloss} + m_{cylinderinlet}T_{cylinderinlet}\alpha_V v\frac{dp_{cylinderinlet}}{d\tau} \end{array} \right\} \tag{6}$$

$$\frac{dT_{cylinderoutlet}}{d\tau}=\frac{1}{c_{cylinder}m_{cylinderoutlet}}*$$

$$\left\{\begin{array}{c}\rho_{oil}Q_{inleak_{cy}}\left[\begin{array}{c}c_{cylinder}\left(T_{cylinderinlet}-T_{cylinderoutlet}\right)\\+\left(1-\frac{\alpha_V\left(T_{cylinderoutlet}+T_{cylinderinlet}\right)}{2}\right)\\*\bar{v}\left(p_{cylinderinlet}-p_{cylinderoutlet}\right)\end{array}\right]\\-h_{cylindershell}A_{cylinderoutlet}\left(T_{cylinderoutlet}-T_{cylindershell}\right)\\+P_{mloss}+m_{cylinderoutlet}T_{cylinderoutlet}\alpha_V v\frac{dp_{cylinderoutlet}}{d\tau}\end{array}\right\} \quad (7)$$

$$\frac{dT_{cylindershell}}{d\tau}=\frac{1}{c_{cylindershell}m_{cylindershell}}*$$

$$\left[\begin{array}{c}h_{cylindershell}A_{cylinderoutlet}\left(T_{cylinderoutlet}-T_{cylindershell}\right)\\+h_{cylindershell}A_{cylinderinlet}\left(T_{cylinderinlet}-T_{cylindershell}\right)\\-h_{cylinderamt}A_{cylinderamt}\left(T_{cylindershell}-T_{amt}\right)\\-\varepsilon A_{cylinderamt}\sigma\left(T_{cylindershell}^4-T_{amt}^4\right)\end{array}\right] \quad (8)$$

The solenoid valve (2-1) in fig. 1 involves 2-1-inlet node, 2-1-outlet node and 2-1-shell node. The solenoid valve (2-2) includes 2-2-inlet node, 2-2-outlet node and 2-2-shell node. The modelling principle of two solenoid valves is same, following eq. (9-11):

$$\frac{dT_{valveinlet}}{d\tau}=\frac{1}{c_{valve}m_{valveinlet}}*$$

$$\left\{\begin{array}{c}\rho_{oil}\left(Q_{th}-Q_{inleak_p}-Q_{exleak_p}\right)\\\left[\begin{array}{c}c_{valve}(T_{outlet}-T_{valveinlet})\\+\left(1-\frac{\alpha_V(T_{outlet}+T_{valveinlet})}{2}\right)\bar{v}(p_{outlet}-p_{valveinlet})\end{array}\right]\\-h_{valveshell}A_{valveshell}(T_{valveinlet}-T_{valveshell})\\+m_{valveinlet}T_{valveinlet}\alpha_V v\frac{dp_{valveinlet}}{d\tau}\end{array}\right\} \quad (9)$$

$$\frac{dT_{valveoutlet}}{d\tau}=\frac{1}{c_{valve}m_{valveoutlet}}*$$

$$\left\{\begin{array}{c}\rho_{oil}\left(Q_{th}-Q_{inleak_p}-Q_{exleak_p}\right)\\\left[\begin{array}{c}c_{valve}(T_{valveinlet}-T_{valveoutlet})+\\\left(1-\frac{\alpha_V(T_{outlet}+T_{valveinlet})}{2}\right)\bar{v}(p_{valveinlet}-p_{valveoutlet})\end{array}\right]\\-h_{valveshell}A_{valveshell}(T_{valveoutlet}-T_{valveshell})\\+P_{minorloss}+m_{valveoutlet}T_{valveoutlet}\alpha_V v\frac{dp_{valveoutlet}}{d\tau}\end{array}\right\} \quad (10)$$

$$\frac{dT_{valveshell}}{d\tau}=\frac{1}{c_{valveshell}m_{valveshell}}*$$

$$\left[\begin{array}{c}h_{valveshell}A_{valveshell}(T_{valveinlet}-T_{valveshell})\\+h_{valveshell}A_{valveshell}(T_{valveoutlet}-T_{valveshell})\\-h_{valveamt}A_{valveamt}(T_{valveshell}-T_{amt})\end{array}\right] \quad (11)$$

PMSM (5) only has two nodes, 5-interior node and 5-shell node as the following eq. (12) and eq. (13):

$$\frac{dT_{motor}}{d\tau}=\frac{1}{c_{motor}m_{motor}}*$$

$$\left[\begin{array}{c}P_{motorloss}-\frac{\lambda A_{motorshell}(T_{motor}-T_{motorshell})}{\delta}\\-\varepsilon A_{motorshell}\sigma(T_{motor}^4-T_{motorshell}^4)\end{array}\right] \quad (12)$$

$$\frac{dT_{motorshell}}{d\tau}=\frac{1}{c_{motorshell}m_{motorshell}}*$$

$$\left[\begin{array}{c}\frac{\lambda A_{motorshell}(T_{motor}-T_{motorshell})}{\delta}\\+\varepsilon A_{motorshell}\sigma(T_{motor}^4-T_{motorshell}^4)\\-h_{motorshellamt}A_{motorshellamt}(T_{motorshell}-T_{amt})\\-\varepsilon A_{motorshellamt}\sigma(T_{motorshell}^4-T_{amt}^4)\end{array}\right] \quad (13)$$

The axial piston pump/motor (6) is comprised of 6-inlet node, 6-outlet node, 6-leakage node and 6-shell node, as the following eq. (14-17):

$$\frac{dT_{inlet}}{d\tau}=\frac{1}{c_{pump}m_{inlet}}*$$

$$\left\{\begin{array}{c}\rho_{oil}Q_{inleak_p}\\\left[\begin{array}{c}c_{pump}(T_{outlet}-T_{inlet})\\+\left(1-\frac{\alpha_V(T_{outlet}+T_{inlet})}{2}\right)\bar{v}(p_{outlet}-p_{inlet})\end{array}\right]\\+\rho_{oil}\left(Q_{th}-Q_{inleak_p}-Q_{outleak_p}-Q_{inleak_{cy}}\right)\\\left[\begin{array}{c}c_{pump}(T_{valveoutlet}-T_{inlet})\\+\left(1-\frac{\alpha_V(T_{valveoutlet}+T_{inlet})}{2}\right)\bar{v}(p_{lrvalveoutlet}-p_{inlet})\end{array}\right]\\+\rho_{oil}Q_{acc}\left[\begin{array}{c}c_{pump}(T_{acc}-T_{inlet})\\+\left(1-\frac{\alpha_V(T_{inlet}+T_{acc})}{2}\right)\bar{v}(p_{acc}-p_{inlet})\end{array}\right]\\+m_{inlet}T_{inlet}\alpha_V v\frac{dp_{inlet}}{d\tau}\end{array}\right\} \quad (14)$$

$$\frac{dT_{outlet}}{d\tau}=\frac{1}{c_{pump}m_{outlet}}*$$

$$\left\{\begin{matrix}\rho_{oil}Q_{th}\begin{bmatrix}c_{pump}(T_{inlet}-T_{outlet})\\+\left(1-\frac{\alpha_V(T_{outlet}+T_{inlet})}{2}\right)\bar{v}(p_{inlet}-p_{outlet})\end{bmatrix}\\+P_{mhloss}+m_{outlet}T_{outlet}\alpha_V v\frac{dp_{outlet}}{d\tau}\end{matrix}\right\}$$

(15)

$$\frac{dT_{leak}}{d\tau}=\frac{1}{c_{pump}m_{leak}}*$$

$$\left\{\begin{matrix}\rho_{oil}Q_{exleak_p}*\\\begin{bmatrix}c_{pump}(T_{outlet}-T_{leak})\\+\left(1-\frac{\alpha_V(T_{outlet}+T_{leak})}{2}\right)\bar{v}(p_{outlet}-p_{leak})\end{bmatrix}\\+P_{chnloss}-h_{pumpshell}A_{pumpshell}(T_{leak}-T_{pumpshell})\\+m_{leak}T_{leak}\alpha_V v\frac{dp_{leak}}{d\tau}\end{matrix}\right\}$$

(16)

$$\frac{dT_{pumpshell}}{d\tau}=\frac{1}{c_{pumpshell}m_{pumpshell}}*$$

$$\begin{bmatrix}h_{pumpshell}A_{pumpshell}(T_{leak}-T_{pumpshell})\\-h_{accpump}A_{accpump}(T_{pumpshell}-T_{acc})\end{bmatrix}$$

(17)

The accumulator (8) contains 8-interior node and 8-shell node as the following eq. (18) and eq. (19). There is a noteworthy change in the equation for one node as the mass of flow entering the accumulator might not be equal to that leaving the accumulator, which means that eq. (2) should be taken into account.

$$\frac{dT_{acc}}{d\tau}=\frac{1}{c_{acc}m_{acc}}*$$

$$\left\{\begin{matrix}\rho_{oil}Q_{exleak_p}\begin{bmatrix}c_{acc}(T_{leak}-T_{acc})\\+\left(1-\frac{\alpha_V(T_{leak}+T_{acc})}{2}\right)\bar{v}(p_{leak}-p_{acc})\end{bmatrix}\\-\rho_{oil}Q_{acc}\begin{pmatrix}c_{acc}(T_{inlet}-T_{acc})\\+\left(1-\frac{\alpha_V(T_{inlet}+T_{acc})}{2}\right)\bar{v}(p_{inlet}-p_{acc})\end{pmatrix}\\-h_{accshell}A_{accshell}(T_{acc}-T_{accshell})\\+h_{accpump}A_{accpump}(T_{pumpshell}-T_{acc})\\+m_{acc}T_{acc}\alpha_V v\frac{dp_{acc}}{d\tau}\end{matrix}\right\}$$

(18)

$$\frac{dT_{accshell}}{d\tau}=\frac{1}{c_{accshell}m_{accshell}}*$$

$$\begin{bmatrix}h_{accshell}A_{accshell}(T_{acc}-T_{accshell})\\-h_{accamt}A_{accamt}(T_{accshell}-T_{amt})\\-\varepsilon A_{accamt}\sigma(T_{accshell}^4-T_{amt}^4)\end{bmatrix}$$

(19)

Expressions of temperature differential equations on the basis of heat transfer in fig. 3 are:

The symmetric cylinder (1), solenoid valve (2-1), (2-2) and PMSM (5) in fig. 1 have the same equations as eq. (6-13). Therefore, equations that are different from those in typical mode are given. CBV (3-1) includes 3-1-inlet node, 3-1-outlet node and 3-1-shell node. CBV (3-2) contains 3-2-inlet node, 3-2-outlet node and 3-2-shell node, following eq. (20-22):

$$\frac{dT_{cbvinlet}}{d\tau}=\frac{1}{c_{cbv}m_{cbvinlet}}*$$

$$\left\{\begin{matrix}\rho_{oil}\left(Q_{th}-Q_{inleak_p}-Q_{exleak_p}-Q_{inleak_{cy}}\right)*\\\begin{bmatrix}c_{cbv}(T_{cylinderoutlet}-T_{cbvinlet})\\+\left(1-\frac{\alpha_V(T_{cylinderoutlet}+T_{cbvinlet})}{2}\right)\\\bar{v}(p_{cylinderoutlet}-p_{cbvinlet})\end{bmatrix}\\-h_{cbvshell}A_{cbvshell}(T_{cbvinlet}-T_{cbvshell})\\+m_{cbvinlet}T_{cbvinlet}\alpha_V v\frac{dp_{cbvinlet}}{d\tau}\end{matrix}\right\}$$

(20)

$$\frac{dT_{cbvoutlet}}{d\tau}=\frac{1}{c_{cbv}m_{cbvoutlet}}*$$

$$\left\{\begin{matrix}\rho_{oil}\left(Q_{th}-Q_{inleak_p}-Q_{exleak_p}-Q_{inleak_{cy}}\right)*\\\begin{bmatrix}c_{cbv}(T_{cbvinlet}-T_{cbvoutlet})+\\\left(1-\frac{\alpha_V(T_{cylinderoutlet}+T_{cbvinlet})}{2}\right)\\\bar{v}(p_{cbvinlet}-p_{cbvoutlet})\end{bmatrix}\\-h_{cbvshell}A_{cbvshell}(T_{cbvoutlet}-T_{cbvshell})\\+P_{minorloss}+m_{cbvoutlet}T_{cbvoutlet}\alpha_V v\frac{dp_{cbvoutlet}}{d\tau}\end{matrix}\right\}$$

(21)

$$\frac{dT_{cbvshell}}{d\tau}=\frac{1}{c_{cbvshell}m_{cbvshell}}*$$

$$\begin{bmatrix}h_{cbvshell}A_{cbvshell}(T_{cbvinlet}-T_{cbvshell})\\+h_{cbvshell}A_{cbvshell}(T_{cbvoutlet}-T_{cbvshell})\\-h_{cbvamt}A_{cbvamt}(T_{cbvshell}-T_{amt})\end{bmatrix}$$

(22)

The axial piston pump/motor (6) is as the following eq. (23-26):

$$\frac{dT_{inlet}}{d\tau}=\frac{1}{c_{pump}m_{inlet}}*$$

$$\begin{bmatrix} \rho_{oil}Q_{inleak_p} * \\ \begin{pmatrix} c_{pump}(T_{outlet}-T_{inlet}) \\ +\left(1-\frac{\alpha_V(T_{outlet}+T_{inlet})}{2}\right)\bar{v}(p_{outlet}-p_{inlet}) \end{pmatrix} \\ +\rho_{oil}Q_{acc}\begin{pmatrix} c_{pump}(T_{acc}-T_{inlet}) \\ +\left(1-\frac{\alpha_V(T_{acc}+T_{inlet})}{2}\right)\bar{v}(p_{acc}-p_{inlet}) \end{pmatrix} \\ +m_{inlet}T_{inlet}\alpha_V v\frac{dp_{inlet}}{d\tau} \end{bmatrix} \tag{23}$$

$$\frac{dT_{outlet}}{d\tau}=\frac{1}{c_{pump}m_{outlet}} * \begin{bmatrix} \rho_{oil}Q_{th}\begin{pmatrix} c_{pump}(T_{inlet}-T_{outlet}) \\ +\left(1-\frac{\alpha_V(T_{outlet}+T_{inlet})}{2}\right)\bar{v}(p_{inlet}-p_{outlet}) \end{pmatrix} \\ +P_{mhloss}+m_{outlet}T_{outlet}\alpha_V v\frac{dp_{outlet}}{d\tau} \end{bmatrix} \tag{24}$$

$$\frac{dT_{leak}}{d\tau}=\frac{1}{c_{pump}m_{leak}} * \begin{bmatrix} \rho_{oil}Q_{exleak_p} * \\ \begin{pmatrix} c_{pump}(T_{outlet}-T_{leak}) \\ +\left(1-\frac{\alpha_V(T_{outlet}+T_{leak})}{2}\right)\bar{v}(p_{outlet}-p_{leak}) \end{pmatrix} \\ +P_{chnloss}-h_{pumpshell}A_{pumpshell}\left(T_{leak}-T_{pumpshell}\right) \\ +m_{leak}T_{leak}\alpha_V v\frac{dp_{leak}}{d\tau} \end{bmatrix} \tag{25}$$

$$\frac{dT_{pumpshell}}{d\tau}=\frac{1}{c_{pumpshell}m_{pumpshell}} * \begin{bmatrix} h_{pumpshell}A_{pumpshell}\left(T_{leak}-T_{pumpshell}\right) \\ -h_{accpump}A_{accpump}\left(T_{pumpshell}-T_{acc}\right) \end{bmatrix} \tag{26}$$

Equation (27-28) about the accumulator (8) are expressed as:

$$\frac{dT_{acc}}{d\tau}=\frac{1}{c_{acc}m_{acc}} * \begin{bmatrix} \rho_{oil}\left(Q_{th}-Q_{inleak_p}-Q_{exleak_p}-Q_{inleak_{cy}}\right) \\ \begin{pmatrix} c_{acc}(T_{cbvoutlet}-T_{acc}) \\ +\left(1-\frac{\alpha_V(T_{cbvoutlet}+T_{acc})}{2}\right)\bar{v}(p_{cbvoutlet}-p_{acc}) \end{pmatrix} \\ +\rho_{oil}Q_{exleak_p}\begin{pmatrix} c_{acc}(T_{leak}-T_{acc}) \\ +\left(1-\frac{\alpha_V(T_{leak}+T_{acc})}{2}\right)\bar{v}(p_{leak}-p_{acc}) \end{pmatrix} \\ -\rho_{oil}Q_{acc}\begin{pmatrix} c_{acc}(T_{inlet}-T_{acc}) \\ +\left(1-\frac{\alpha_V(T_{inlet}+T_{acc})}{2}\right)\bar{v}(p_{inlet}-p_{acc}) \end{pmatrix} \\ -h_{accshell}A_{accshell}(T_{acc}-T_{accshell}) \\ +h_{accpump}A_{accpump}\left(T_{pumpshell}-T_{acc}\right) \\ +m_{acc}T_{acc}\alpha_V v\frac{dp_{acc}}{d\tau} \end{bmatrix} \tag{27}$$

$$\frac{dT_{accshell}}{d\tau}=\frac{1}{c_{accshell}m_{accshell}} * \begin{bmatrix} h_{accshell}A_{accshell}(T_{acc}-T_{accshell}) \\ -h_{accamt}A_{accamt}(T_{accshell}-T_{amt}) \\ -\varepsilon A_{accamt}\sigma(T_{accshell}^4-T_{amt}^4) \end{bmatrix} \tag{28}$$

4 Simulation results

According to fig. 5, dynamic performance of the EHA is simulated through AMESim as one part of the co-simulation, and PID controller is deployed. In order to estimate thermal behavior, two thermal models are developed in MATLAB/Simulink for each operating mode.

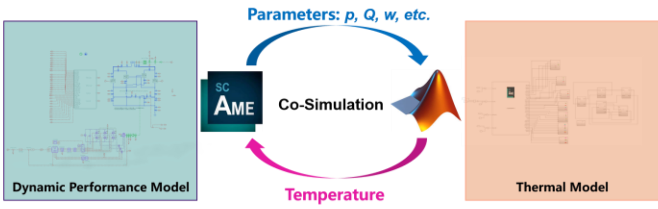

Figure 5: Data exchange within co-simulation

The EHA achieves rod extension and retraction by driving the pump in different rotational directions. Consequently, although the mathematical temperature differential equations are derived, it is crucial that the Simulink model accurately accounts for directional parameters when data is transferred from AMESim.

4.1 Duty cycle

Since this EHA is designed for lifting applications, it consistently sustains force in a single direction, which means the EHA operates in two quadrants. As shown in fig. 6(a), the load force is obtained from Mevea-based simulations[22] and subsequently scaled down and linearized to align with the specifications of the integrated EHA.

Figure. 6(b) illustrates the trajectory of a hybrid wheel loader completing a single and 60-second duty cycle, as viewed from Mevea user interface. This duty cycle represents a typical loading and unloading process. The sequence begins with the wheel loader moving from point A to point B without a load. Upon reaching point C, the loader lowers its bucket, tilts it, and raises the boom to collect material into the bucket. After loading, the loader reverses to point D, then drives forward to point E to unload the material. The cycle is completed when the loader returns to the starting position at point A.

The stroke of the cylinder is also scaled down. Even though models of dual operating modes in AMESim employ three-loop PID controllers, they have varied control parameters and effects due to different working hydraulic components. Figure. 6(c) and (d) presents a comparison of piston position dynamics as a function of time between a reference command and a simulated response. The most notable discrepancy occurs around point C, where the piston continues to retract in fig. 6(c) because of a sharp increase in load force, as depicted in fig. 6(a). This sudden load boom exceeds the hydraulic system's damping to counteract the impact in real-time, resulting in a pronounced deviation in the response. Nevertheless, CBVs play an important role in resisting this impact in safety mode, which can be proved by the curve around point C in fig. 6(d).

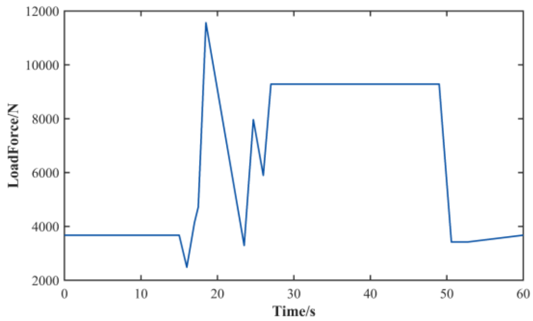

(a) Load in one duty cycle

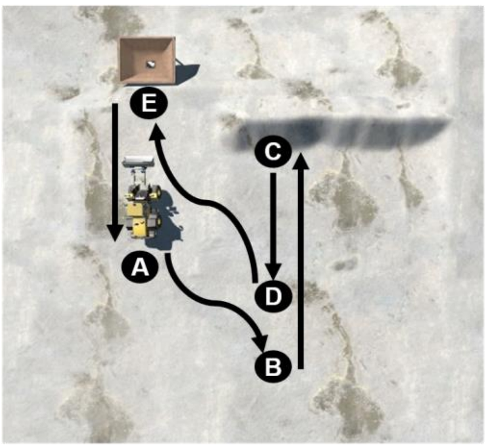

(b) Trajectory of the hybrid wheel loader

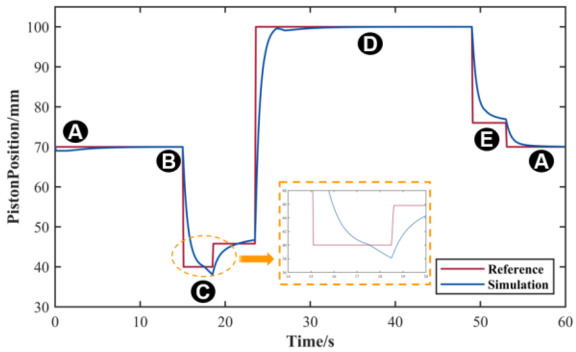

(c) Comparison between reference and simulation results under typical mode

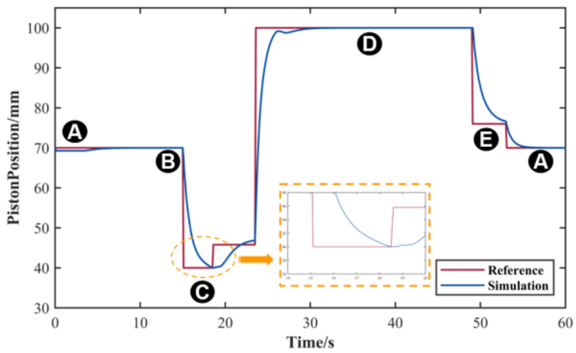

(d) Comparison between reference and simulation results under safety mode

Figure 6: Duty cycle of the hybrid wheel loader under two modes

Initial temperatures of all components are set to 20.00 ℃ (293.15 K), matching the ambient temperature, which remains constant at 20.00 ℃ throughout the process. To intuitively observe the temperature trend, a co-simulation was conducted with a 60-second duty cycle and repeated a total duration of 3600 seconds.

4.2 Temperature results

Temperature in 6-inlet node under safety mode is a little larger than that under typical mode. The temperature of 6-outlet node in safety mode in fig. 7(b) closely follow that in typical mode in fig. 7(a). On the contrary, the temperatures of 6-leakage node and 6-shell node in typical mode are significantly higher than those in safety mode, with the difference becoming more pronounced as time progresses. A critical observation from fig. 7 is that in typical mode, the temperature in 6-shell node curve gradually rises above the 6-outlet node temperature after approximately 1500 seconds. Nonetheless, in safety mode, the 6-shell node temperature consistently remains lower than the 6-outlet node temperature throughout the entire duration.

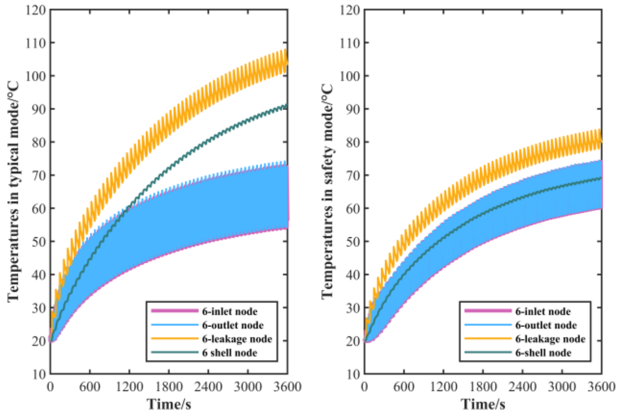

(a) typical mode *(b) safety mode*

Figure 7: Temperatures in the pump under dual modes

As mentioned in Chapters 2 and 4, the inlet and outlet ports of a pump switch roles as the flow direction changes. This presents two possible approaches for implementation in MATLAB/Simulink. The first approach defines the two pump ports as Port A and Port B, where each port can function as either an inlet port or an outlet port. Consequently, each port requires two distinct states (represented by two separate equations, such as eq. (14) and eq. (15)) that must switch accordingly. However, this method is challenging to implement in software.

The second approach assigns that the inlet port is either Port A or Port B, requiring only parameter switching within a single equation while inheriting temperature from the previous state. This study adopts the second approach, though it results in significant temperature oscillations during switching.

In spite of different modes, temperatures of 5-interior node and 5-shell node are quite similar respectively as fig. 8 shows.

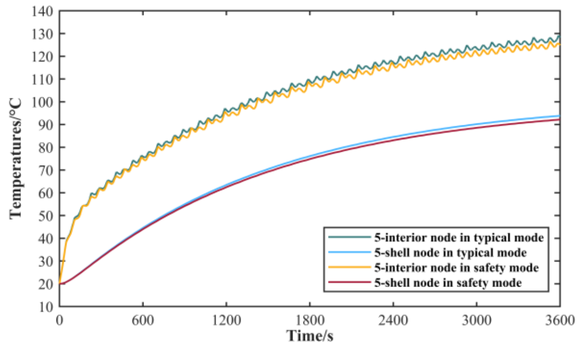

Figure 8: Temperatures in the PMSM under dual modes

Figure. 9 clearly demonstrates that the temperatures of the three CBV (3-2) nodes—the inlet, outlet, and shell nodes—are varied, with 3-2-outlet node temperature being the highest. Conversely, the temperatures of the 3-1-inlet and 3-1-outlet nodes remain nearly identical, exhibiting no distinguishable difference throughout the observed period.

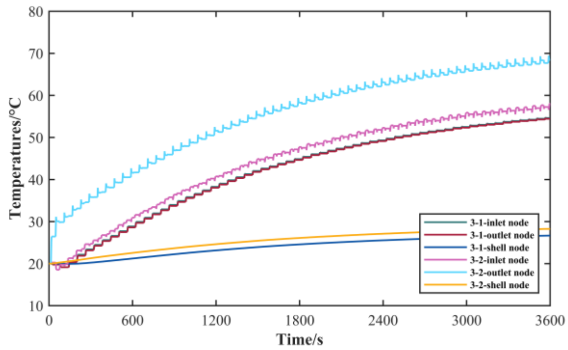

Figure 9: Temperatures in the CBV under safety mode

Table. 1 shows temperatures of all nodes at 3600 seconds for typical mode and safety mode. It is evident that the cylinder (1), solenoid valve (2-1) and (2-2), and exhibit higher temperatures in safety mode, compared to typical mode. In contrast, temperatures at the 8-interior node and 8-shell node are lower in safety mode than those in typical mode.

Table 1 Final Temperatures at the 3600 seconds

Typical mode		**Safety mode**	
Node Name	**Temperature**	**Node Name**	**Temperature**
1-inlet	42.99 ℃	1-inlet	68.29 ℃
1-outlet	37.97 ℃	1-outlet	54.79 ℃
1-shell	36.22 ℃	1-shell	49.08 ℃
2-1-inlet	42.01 ℃	2-1-inlet	72.16 ℃
2-1-outlet	50.56 ℃	2-1-outlet	73.17 ℃
2-1-shell	26.12 ℃	2-1-shell	30.33 ℃
2-2 inlet	46.29 ℃	2-2 inlet	73.08 ℃
2-2-outlet	55.89 ℃	2-2-outlet	73.25 ℃
2-2-shell	27.24 ℃	2-2-shell	30.26 ℃
5-interior	128.26 ℃	5-interior	124.85 ℃
5-shell	93.88 ℃	5-shell	92.20 ℃
6-inlet	54.41 ℃	6-inlet	60.24 ℃
6-outlet	72.44 ℃	6-outlet	74.01 ℃
6-leakage	105.82 ℃	6-leakage	82.06 ℃
6-shell	91.24 ℃	6-shell	69.18 ℃
8-interior	81.13 ℃	8-interior	60.64 ℃
8-shell	72.05 ℃	8-shell	54.35 ℃
		3-1-inlet	74.35 ℃
		3-1-outlet	74.67 ℃
		3-1-shell	30.35 ℃
		3-2-inlet	57.25 ℃
		3-2-outlet	67.70 ℃
		3-2-shell	28.25 ℃

5 Analysis and discussion

There are two possible reasons to explain that the difference in PMSM temperatures between the modes appears surprisingly low: 1. Imprecise simulating values. We haven't done experiments to correct a few of coefficients; 2. In typical mode, PMSM must work in the situation of high torque and low speed when the piston reaches the desired position. In this case, PMSM keeps rotating and generating heat. In safety mode, motor needs more power to drive pump and then open CBVs.

The higher temperatures observed in the cylinder during safety mode can be attributed to the behavior of the CBVs. In safety mode, CBVs prevent fluid flow until the pressure inside the cylinder's chamber reaches a sufficient level to open the valve. On the contrary, in typical mode, fluid flows through the solenoid valve without any restriction. When the piston reaches necessary position, CBVs can assist in maintaining the load without the pump working with small flow rate and high torque. This is the reason why the temperature of pump leakage node in safety mode is lower than in typical mode in fig. 7. Additionally, since the pump is submerged in oil within the accumulator, the pump shell struggles to dissipate heat effectively to the ambient air as the oil temperature increases. However, in safety mode, more fluid enters the accumulator through the CBVs, enhancing convective heat transfer. This results in lower temperature in the pump shell node in safety mode in comparison to the outlet node. Similarly, this enhanced heat transfer explains why the temperatures of accumulator's two nodes are lower in safety mode than in typical mode.

Furthermore, this EHA used for lifting experiences a continuous pushing force, even when the bucket is unloaded, leading to higher pressure in one chamber of the cylinder. The pilot pressure required to open the CBV closely matches the lower pressure in the other chamber. These factors result in discontinuous fluid flow through one of the CBVs when the pilot pressure is insufficiently high. Consequently, varying temperatures are observed at the CBV's inlet and outlet, as illustrated in fig. 9 via curves of temperature rise of the 3-2-inlet node and 3-2-outlet node.

These results indicate a difference in thermal behavior between the two modes, highlighting the influence of mode-specific conditions on system temperature distribution.

6 Conclusion

This study has demonstrated the viability of a dual-mode integrated EHA as a direct replacement for the conventional lift cylinder in hybrid wheel loaders, fully satisfying ISO 8643 safety requirements. Lumped parameter thermal models for both open and closed hydraulic circuits were developed and validated via co-simulation in AMESim and MATLAB Simulink over a representative 3,600 s duty cycle.

Results indicate that engaging the CBVs under safety mode markedly enhances load-holding capacity and enables reliable two-quadrant operation under variable loads. However, intermittent fluid flow in this mode elevates cylinder and solenoid valve temperatures, increasing localized thermal stress, even as convective heat transfer in the pump and accumulator is improved.

In contrast, EHA under typical mode (CBVs disengaged) maintains continuous fluid circulation, which keeps cylinder and valve temperatures lower but shifts the bulk of thermal load to the pump leakage node and the accumulator. Notably, permanent-magnet synchronous motor temperatures remained statistically unchanged between both modes, highlighting the motor's inherent thermal robustness.

Based on these findings, we recommend targeted cooling strategies for each mode: focused heat dissipation for the cylinder and valves during safety-mode operation, and enhanced pump-leakage and accumulator heat rejection in typical mode. Overall, the proposed modeling and simulation framework offers a clear pathway for optimizing component-level thermal management in electrified hydraulic systems, paving the way for future work on transient control integration and advanced heat-exchanger design to further boost efficiency and reliability in non-road mobile machinery.

Future work: The primary objective is to conduct experiments to refine parameters and validate the models. The testrig is being built and is equipped with a real-time simulation machine for Hardware-in-the-Loop (HIL) simulation.

Acknowledgements

This research is supported by international joint doctoral education fund of Beihang University. Also, thanks for the help from Prof. Tatiana Minav.

Nomenclature

Designation	Denotation	Unit
$\dot{Q}$	Rate of heat transfer	W
$\dot{W}$	Rate of work	W
$\dot{m}$	Mass flow rate	kg/s
u	Specific internal energy	J/kg
v	Specific volume	m^3/kg
$\bar{v}$	Average specific volume	m^3/kg
p	Fluid pressure	Pa
ρ	Fluid density	kg/m^3
ε	Emissivity	1
σ	Stefan-Boltzmann constant	W/(m^2·K^4)
λ	Thermal conductivity	W/(m·K)
δ	Thickness	m
k_e	Specific kinetic energy	J/kg
p_e	Specific potential energy	J/kg
α_v	Coefficient of cubic expansion	1/K
E_{CM}	Control mass energy	J

Q	Volumetric flow rate	m^3/s
T	Temperature	K
τ	Time	second
P_{mloss}	Mechanical loss in cylinder	W
$P_{minorloss}$	Energy loss in valve	W
$P_{motorloss}$	Energy loss in Motor	W
P_{mhloss}	Mechanical loss in pump	W
$P_{chnloss}$	Churning loss in pump	W

References

[1] R. Hagan *et al.*, 'Non-Road Mobile Machinery Emissions and Regulations: A Review', *Air*, vol. 1, no. 1, Art. no. 1, Mar. 2023, doi: 10.3390/air1010002.

[2] B. Singh, 'Novel and Ruggedized Power Electronics for Off-Highway Vehicles', *IEEE Electrification Magazine*, vol. 2, no. 2, pp. 31–41, Jun. 2014, doi: 10.1109/MELE.2014.2313157.

[3] M. de F. Ramos, D. A. de L. Brandao, D. P. V. Galo, B. de J. Cardoso Filho, I. A. Pires, and T. A. C. Maia, 'A Study on the Performance of the Electrification of Hydraulic Implements in a Compact Non-Road Mobile Machine: A Case Applied to a Backhoe Loader', *World Electric Vehicle Journal*, vol. 15, no. 4, Art. no. 4, Apr. 2024, doi: 10.3390/wevj15040127.

[4] S. Hui and J. Junqing, 'Research on the system configuration and energy control strategy for parallel hydraulic hybrid loader', *Automation in Construction*, vol. 19, no. 2, pp. 213–220, Mar. 2010, doi: 10.1016/j.autcon.2009.10.006.

[5] M. Ochiai and S. Ryu, 'Hybrid in Construction Machinery', *Proceedings of the JFPS International Symposium on Fluid Power*, vol. 2008, no. 7–1, pp. 41–44, 2008, doi: 10.5739/isfp.2008.41.

[6] N. Zou *et al.*, 'Series-parallel hybrid power loader', CN102653228A, Sep. 05, 2012 Accessed: May 16, 2024. [Online]. Available: https://patents.google.com/patent/CN102653228A/en

[7] M. Axin, *Fluid power systems for mobile applications: with a focus on energy efficiency and dynamic characteristics*. Linköping: Linköping University, Department of Management and Engineering, 2013.

[8] S. Ketelsen, D. Padovani, T. O. Andersen, M. K. Ebbesen, and L. Schmidt, 'Classification and Review of Pump-Controlled Differential Cylinder Drives', *Energies*, vol. 12, no. 7, Art. no. 7, Jan. 2019, doi: 10.3390/en12071293.

[9] S. H. Cho and R. Burton, 'Position control of high performance hydrostatic actuation system using a simple adaptive control (SAC) method', *Mechatronics*, vol. 21, no. 1, pp. 109–115, Feb. 2011, doi: 10.1016/j.mechatronics.2010.09.003.

[10] Y. Shang *et al.*, 'A Novel Electro Hydrostatic Actuator System With Energy Recovery Module for More Electric Aircraft', *IEEE Transactions on Industrial Electronics*, vol. 67, no. 4, pp. 2991–2999, Apr. 2020, doi: 10.1109/TIE.2019.2905834.

[11] Z. Lin, Z. Lin, F. Wang, and B. Xu, 'A series electric hybrid wheel loader powertrain with independent electric load-sensing system', *Energy*, vol. 286, p. 129497, Jan. 2024, doi: 10.1016/j.energy.2023.129497.

[12] Y. Qiao, J. Wu, F. Wang, and B. Xu, 'Electro-Hydrostatic Actuator System With Separate Design to Improve Efficiency for Working Function of Electric Wheel Loader', in *BATH/ASME 2024 Symposium on Fluid Power and Motion Control*, Bath, United Kingdom: American Society of Mechanical Engineers, Sep. 2024, p. V001T01A033. doi: 10.1115/FPMC2024-141117.

[13] D. Fassbender and T. Minav, 'An Algorithm for the Broad Evaluation of Potential Matches between Actuator Concepts and Heavy-Duty Mobile Applications', *Actuators*, vol. 10, no. 6, Art. no. 6, Jun. 2021, doi: 10.3390/act10060111.

[14] ISO Standard No.8643: 2017.

[15] J. Andersson, P. Krus, K. Nilsson, and K. Storck, 'MODELLING AND SIMULATION OF HEAT GENERATION IN ELECTRO-HYDROSTATIC ACTUATION SYSTEMS', *Proceedings of the JFPS International Symposium on Fluid Power*, vol. 1999, no. 4, pp. 537–542, 1999, doi: 10.5739/isfp.1999.537.

[16] S. Michel, 'Prediction of the thermo-energetic behaviour of an electrohydraulic compact drive', Mar. 2016.

[17] S. Fan *et al.*, 'Thermal analysis of key components in EHA system under high temperature condition', in *CSAA/IET International Conference on Aircraft Utility Systems (AUS 2022)*, Aug. 2022, pp. 1179–1184. doi: 10.1049/icp.2022.1837.

[18] T. Minav, L. Papini, and M. Pietola, 'A Thermal analysis of Direct Driven Hydraulics', Mar. 2016.

[19] T. Minav, J. Heikkinen, T. Schimmel, and M. Pietola, 'Direct Driven Hydraulic Drive: Effect of Oil on Efficiency in Sub-Zero Conditions', *Energies*, vol. 12, no. 2, p. 219, Jan. 2019, doi: 10.3390/en12020219.

[20] X. Han, T. Minav, M. Wang, Y. Fu, and M. Pietola, 'Thermal Coupling Simulation of Electro-Hydrostatic Actuator Subjected to Critical Temperature Conditions', *TJFP*, Sep. 2022, doi: 10.13052/ijfp1439-9776.2336.

[21] J. A. Sidders, D. G. Tilley, and P. J. Chappie, 'Thermal-Hydraulic Performance Prediction in Fluid Power Systems', *Proceedings of the Institution of Mechanical Engineers, Part I: Journal of Systems and Control Engineering*, vol. 210, no. 4, pp. 231–242, Nov. 1996, doi: 10.1243/PIME_PROC_1996_210_462_02.

[22] 'Training Simulators for Construction Equipment | Mevea Digital Twins', Mevea. Accessed: May 07, 2025. [Online]. Available: https://mevea.com/solutions/training-simulators/construction-equipment/